Published in final edited form as:
J Neural Eng. 2011 August ; 8(4): 046017. doi:10.1088/1741-2560/8/4/046017.

A cortical neural prosthesis for restoring and enhancing memory

Theodore W Berger[1], **Robert E Hampson**[2], **Dong Song**[1], **Anushka Goonawardena**[2], **Vasilis Z Marmarelis**[1], and **Sam A Deadwyler**[2]

[1] Depatment of Biomedical Engineering, University of Southern California, Los Angeles, CA, USA

[2] Department of Physiology and Pharmacology, Wake Forest University, Winston-Salem, NC, USA

Abstract

A primary objective in developing a neural prosthesis is to replace neural circuitry in the brain that no longer functions appropriately. Such a goal requires artificial reconstruction of neuron-to-neuron connections in a way that can be recognized by the remaining normal circuitry, and that promotes appropriate interaction. In this study, the application of a specially designed neural prosthesis using a multi-input/multi-output (MIMO) nonlinear model is demonstrated by using trains of electrical stimulation pulses to substitute for MIMO model derived ensemble firing patterns. Ensembles of CA3 and CA1 hippocampal neurons, recorded from rats performing a delayed-nonmatch-to-sample (DNMS) memory task, exhibited successful encoding of trial-specific sample lever information in the form of different spatiotemporal firing patterns. MIMO patterns, identified online and in real-time, were employed within a closed-loop behavioral paradigm. Results showed that the model was able to predict successful performance on the same trial. Also, MIMO model-derived patterns, delivered as electrical stimulation to the same electrodes, improved performance under normal testing conditions and, more importantly, were capable of recovering performance when delivered to animals with ensemble hippocampal activity compromised by pharmacologic blockade of synaptic transmission. These integrated experimental-modeling studies show for the first time that, with sufficient information about the neural coding of memories, a neural prosthesis capable of real-time diagnosis and manipulation of the encoding process can restore and even enhance cognitive, mnemonic processes.

1. Introduction

The utility and validation of neural prosthetic devices has improved considerably in recent years with several new applications providing relief and improvement from pathological circumstances that affect motor control, locomotion, and restoration of movement (Velliste *et al* 2008, Leuthardt *et al* 2009, Isa *et al* 2009, Wang *et al* 2010a). The primary models for such devices have utilized the well-established assessment of motor cortical neural ensemble firing related to arm movements and brain–computer interfaces (BCIs) for control of scalp recorded neural events correlated with detection of expected sensory events (Daly and Wolpaw 2008, Leuthardt *et al* 2009, Wang *et al* 2010b). While highly successful, the above approaches have only recently been applied to cognitive processes within a context that can be shown to facilitate or restore mental activity impaired by (1) events such as lack of attention to or misinterpretation of critical information in normal subjects (Jarosiewicz *et al* 2008, Legenstein *et al* 2010), or (2) the loss of these capacities due to injury or disease that

sdeadwyl@wfubmc.edu.

affect cortical structures involved in information, encoding, and integration (Moritz *et al* 2008, Miller *et al* 2010).

This paper describes the initial demonstration of a cortical neural prosthesis applied to information processing of two subregions of the hippocampus involved in the formation of long-term memory. These memories were essential for successful performance of a cognitive task requiring encoding and retrieval of information on a trial-by-trial basis. The neural structure tested by the device, the rodent hippocampus, has been extensively characterized with respect its role in performance of a delayed-nonmatch-to-sample (DNMS) working memory task (Deadwyler and Hampson 1995, 1997, 2006, Hampson *et al* 1999b, Hampson and Deadwyler 2003, Deadwyler *et al* 2007) and offline computational assessment of firing relationships during that performance (Song *et al* 2007a, 2007b). Such characterization provided the substrate for online application of the device to extract critical functional processing from ensembles of hippocampal neurons required for the performance of the task (Deadwyler and Hampson 2004, Hampson *et al* 2008), and to establish when not present, information processing necessary for successful completion of the task (Hampson and Deadwyler 2003, Deadwyler *et al* 2007). Here we demonstrate how this prototype of a cortical prosthesis is capable of (1) monitoring the input pattern to hippocampus during the information encoding phase of the task, (2) predicting accurately the associated hippocampal output pattern and the degree of success related to such encoding, and (3) delivering stimulation with electrical pulses during the same phase of the task in a pattern that conforms to the normal firing of the hippocampal output region on successful trials. The utility of this cortical prosthesis is further demonstrated by the capacity to substitute successful encoding stimulation when hippocampal ensembles are compromised and cannot generate the necessary codes to perform the task successfully.

2. Methods

2.1. Subjects and training

Long-Evans rats (Harlan) aged four–six months were used as subjects (n = 45). All animal protocols and surgical procedures are approved by the Wake Forest University Institutional Animal Care and Use Committee and the National Institute of Health Guide for the Care and Use of Laboratory Animals (NIH Publication no 8023). Animals maintained at 85% of *ad libitum* body weight were trained to criterion performance levels in the DNMS task and then implanted bilaterally with two identical array electrodes (Neurolinc, New York, NY), each consisting of two rows of eight stainless steel wires (diameter: 20 μ) positioned parallel to the longitudinal axis of hippocampus (figure 1). The distance between two adjacent electrodes in the array within a row was 200 μm and between rows was 400 μm to conform to the locations of the respective CA3 and CA1 cell layers. The electrode array was lowered to a depth of 3.0–4.0 mm from the cortical surface with the longer electrode row positioned in the CA3 cell layer and shorter row 1.2 mm higher with tips in the CA1 layer. Extracellular neuronal spike activity was monitored during implantation to maximize placement in the appropriate hippocampal cell layers. Animals were allowed to recover from surgery for at least one week before continuing behavioral testing (Hampson *et al* 2008).

2.2. Behavioral apparatus and training procedure

The behavioral testing apparatus for the DNMS task is the same as reported in prior studies (Deadwyler and Hampson 1997, 2004, Hampson *et al* 2008) and consists of a 43 × 43 × 50 cm Plexiglas chamber with two retractable levers (left and right) positioned on either side of a water trough on one wall of the chamber (figure 1). A photocell with a cue light activated nose-poke (NP) device was mounted in the center of the opposite wall. The chamber was housed inside a sound-attenuated cubicle. The DNMS task consisted of three phases: (1)

sample phase: in which a single lever was presented randomly in either the left or right position; when the animal pressed the lever, the event was classified as sample response (SR), (2) delay phase: of variable duration (1–30 s) in which a nosepoke (NP) into a photocell was required to advance to the (3) nonmatch phase: in which both levers were presented and a response on the lever opposite to the SR, i.e., a nonmatch response (NR), was required for delivery of a drop of water (0.4 ml) in the trough. A response in the nonmatch phase on the lever in the same position as the SR (match response) constituted an 'error' with no water delivery and a turning off of the lights in the chamber for 5.0 s. Following the reward delivery (or an error) the levers were retracted for 10.0 s before the sample lever was presented to begin the next trial. Individual performance was assessed as % correct NRs with respect to the total number of trials (100–150) per daily (1–2 h) session.

2.3. Multineuron recording of hippocampal ensembles

Animals were connected by a cable to a 32-channel recording apparatus via a slip-ring commutator (Crist Instruments, Hagerstown, MD) which allowed free movement at all times during behavioral testing. Single neuron action potentials (spikes) were isolated by time-amplitude window discrimination and computer-identified (Plexon Inc., Dallas, TX, USA) by individual waveform characteristics using a multi-neuron acquisition (MAP) processor. Isolated spike waveforms exhibiting firing rates consistent with CA1 and CA3 principal cells (i.e. 0.5–5.0 Hz baseline firing rate) which showed stable behavioral correlates across sessions (Deadwyler *et al* 2007, Deadwyler and Hampson 2006, Hampson *et al* 2008) were employed for experimental manipulations and model development. Hippocampal ensembles used to analyze encoding of DNMP events consisted of 15–32 single neurons, each recorded from a separate identified electrode location on the bilateral arrays (Song *et al* 2007a).

2.4. Nonlinear systems identification of ensemble codes

A general, Volterra kernel-based strategy for modeling multi-input/multi-output (MIMO) nonlinear dynamics underlying spike train-to-spike train transformations between CA3 and CA1 was established to predict output patterns of CA1 firing pattern from input patterns of CA3 neural activity (Berger *et al* 2005, 2010 Song *et al* 2007a, 2009). In this approach, the identification of spatio-temporal pattern transformations from the hippocampal CA3 region to the CA1 region is formulated as the estimation of an MIMO model that can be decomposed into a series of multi-input, single-output (MISO) models with physiologically identifiable structure that can be expressed by the following equations:

$$w=u(k,x)+a(h,y)+\varepsilon(\sigma), \qquad y=\begin{cases} 0 & \text{when } w<\theta \\ 1 & \text{when } w \geq \theta. \end{cases}$$

The variable x represents input spike trains; y represents output spike trains. The hidden variable w represents the pre-threshold membrane potential of the output neurons, and is equal to the summation of three components, i.e. post-synaptic potential u caused by input spike trains, the output spike-triggered after-potential a, and a Gaussian white noise ε with standard deviation σ. The noise term models both intrinsic noise of the output neuron and the contribution of unobserved inputs. When w exceeds threshold, θ, an output spike is generated and a feedback after-potential (a) is triggered and then added to w. Feedforward kernels k describe the transformation from x to u. The feedback kernel, h, describes the transformation from y to a. u can be expressed as a Volterra functional series of x, as in

$$\begin{aligned} u(t) = k_0 &+ \sum_{n=1}^{N}\sum_{\tau=0}^{M_k} k_1^{(n)}(\tau)x_n(t-\tau) \\ &+ \sum_{n=1}^{N}\sum_{\tau_1=0}^{M_k}\sum_{\tau_2=0}^{M_k} k_{2s}^{(n)}(\tau_1,\tau_2)x_n(t-\tau_1)x_n(t-\tau_2) \\ &+ \sum_{n_1=1}^{N}\sum_{n_2=1}^{n_1-1}\sum_{\tau_1=0}^{M_k}\sum_{\tau_2=0}^{M_k} k_{2x}^{(n_1,n_2)}(\tau_1,\tau_2)x_{n_1}(t-\tau_1)x_{n_2}(t-\tau_2) \\ &+ \sum_{n=1}^{N}\sum_{\tau_1=0}^{M_k}\sum_{\tau_1=0}^{M_k}\sum_{\tau_3=0}^{M_k} k_{3s}^{(n)}(\tau_1,\tau_2,\tau_3) \\ &\times x_n(t-\tau_1)x_n(t-\tau_2)x_n(t-\tau_3)+\cdots \end{aligned}$$

The zeroth order kernel, k_0, is the value of u when the input is absent. First order kernels, $k_1^{(n)}$, describe the linear relation between the nth input x_n and u. Second and third order self-kernels, $k_2^{(n)}$, and $k_{3s}^{(n)}$, describe the second and third order nonlinear relation between nth input x_n and u, respectively. Second order cross-kernels $k_{2x}^{(n1,n2)}$ reflect the second order nonlinear interactions between each unique pair of inputs (x_{n1} and x_{n2}) as they affect u. N is the number of inputs. M_k denotes the memory length of the feedforward process. The feedback variable a can be expressed as:

$$a(t) = \sum_{\tau=1}^{M_h} h(\tau)y(t-\tau),$$

where h is the linear feedback kernel. M_h is the memory length of the feedback process. In total, then, the model describes how temporal patterns of third order (i.e., the effects of triplets) for each input, and second order (i.e., the effects of pairs) for any of two interacting inputs, affect each output, taking into account differing noise level and output spike-triggered feedback (the latter due to circuitry and/or membrane biophysics), and neuron-specific differences in thresholds. In order to reduce the number of open parameters to be estimated, both k and h are expanded with orthonormal Laguerre basis functions (Marmarelis and Orme 1993, Marmarelis 2004, Marmarelis and Berger 2005). Due to the Gaussian noise term and the threshold, this model can be considered a special case of the generalized Laguerre–Volterra model (GLVM), which employs a *probit* link function (Song *et al* 2007b, 2009). All model parameters, i.e., feedforward Volterra kernel k and feedback Volterra kernel h can be estimated using an iterative re-weighted least-squares method (Truccolo *et al* 2005). Noise standard deviation σ and threshold θ are redundant variables and thus can be indirectly obtained through variable transformation (Song *et al* 2007b, 2009). Due to the stochastic nature of the system, estimated models are validated using an out-of-sample Kolmogorov–Smirnov test based on the time-rescaling theorem (Brown *et al* 2002).

Prior studies have shown the success of the application of MIMO model (Song *et al* 2007a, 2007b) which was applied offline to data from hippocampal ensemble recordings in the DNMS task to determine the temporal relation between spike occurrences recorded in CA3 and CA1 (Zanos *et al* 2008, Song *et al* 2009). Recent investigations have revealed extension of this capacity to online control of DNMS performance (Hampson *et al* 2011). In the latter case it was revealed that the recordings from the CA3 electrodes constituted the inputs to the model, while the designated outputs were spikes recorded from the CA1 electrodes on the same array (figure 1) which corresponded to the well-established monosynaptic relationship between the two cell populations via Schaffer collateral fiber connections (Witter and Amaral 2004).

2.5. MIMO generated ensemble stimulation

Stimulation studies were conducted with a custom built 16-channel stimulator (Triangle Bio Systems Inc., Durham, NC) designed to deliver patterns of electrical pulses to CA1 electrodes in both (bilateral) hippocampal arrays. Stimulator output was delivered as bipolar pulses, 1.0 ms duration, 0.1–15 V, 20–100 μA to pairs of CA1 electrodes located adjacent to each other on the array (figure 1). This provided maximal isolation of individual pulse trains from other electrodes in the same array and restricted stimulation trains to the regions where the same firing patterns were obtained from CA1 cells recorded on the same electrodes. Stimulation patterns consisted of 16 channels of pulses delivered bipolar to all CA1 electrodes in trains of 1.5–3.0 s duration prior to and during the SR, or for control purposes, shifted to 3.0–7.0 s after the SR. Controls for nonspecific effects of stimulation included (1) shuffling of MIMO coefficients to generate stimulation patterns, or (2) reversing the appropriate pattern for a given lever position to the pattern for the opposite lever position. To test of the effectiveness of the electrical stimulation patterns some animals were prepared with minipumps to infuse the glutamatergic blocking agent MK801 into the hippocampus to disrupt MIMO model predicted output patterns in CA1 indicated by a loss of identified SR codes. The drug was infused chronically (37.5 μg h^{-1}; 1.5 mg ml^{-1}, 0.25 μl h^{-1}) over a two week period in animals that had previously showed facilitated performance on trials with MIMO stimulation delivered during a similar chronic infusion of saline vehicle. The location of the infusion cannula is shown in the illustration of array recordings in figure 1.

3. Results

Prior investigations have demonstrated from online recordings of hippocampal activity that information encoded during the SR and employed in the nonmatch phase is predictive of successful or unsuccessful performance based on the duration of the ensuing delay interval (Deadwyler *et al* 2007, Hampson *et al* 2008). These investigations have determined that the retrieval process (NR) is not as critical as the encoding (SR) phase of the task since errors are correlated more with lack of effective hippocampal cell firing during the SR (Simeral *et al* 2005). DNMS trials are grouped by 5–10 s intervals of delay duration, and plotted as mean (± S.E.M.) percentage of correct trials. Animals were trained on trials with delays of 1–30 s, then subjected on a random infrequent basis to ‘probe’ trials, with delays >30 s, employed to assess accuracy of the MIMO model and closed loop manipulations. Control performance on ‘probe’ trials typically resulted in near ‘chance’ (50% correct) performance and provided a consistent basis for testing the application of the MIMO model and derived patterns of electrical stimulation. The effectiveness or ‘strength’ of the SR encoding process was evaluated with respect to whether the trial was rewarded or not as a result of the choice of the NR. ‘Strong’ SR codes are defined as MIMO derived firing patterns associated with correct responding on long delay trials, while ‘weak’ SR codes are defined as MIMO patterns that occur on error (non-rewarded) trials irrespective of duration of delay. Therefore, performance of the task on a given trial is characterized by (1) an interaction between ‘strength’ of the SR code (i.e. ‘completeness’ of the spatiotemporal firing pattern exhibited on correct long delay trials) for sample lever position and (2) duration of the ensuing delay preceding the nonmatch phase where the encoded SR information is retrieved to perform the NR (figure 1).

3.1. MIMO model measure of SR strength of encoding predicts learned behavior

The method for assessing the relationship between strength of the SR code and performance utilized a closed loop paradigm (figure 2) in which CA3 activity occuring 1.5–3.0 s prior to the SR was used as input to the MIMO model to provide a prediction of the output firing pattern of simultaneously recorded CA1 cells (Hampson *et al* 2011). The strength of the SR code categorized on the basis of correlations with prior performance as defined above was

utilized to adjust the duration of the delay online during the same trial (figure 2). Depiction of differences in strong versus weak SR codes is shown by the mean firing rate contour maps in figure 2 (lower right). Because of the extended time interval between the SR and NR due to interposed delays in the task it was possible to adjust the delay duration on the same trial as a function of the 'strength' of the encoded SR, determined online by the MIMO model. The closed loop procedure adjusted delay duration primarily in two ways: (1) on any trial in the session where a weak SR code was detected the delay was reduced to 10 s, and (2) on trials with detected strong SR codes, delays were extended to 40, 50, or 60 s. The graph in figure 2 (lower left) shows the two extreme conditions of closed loop control of performance by (1) shortening the delay to 10 s for weak SR code trials (CL-weak code) or (2) lengthening the delay to > 30 s when strong SR codes were detected (CL-strong codes). It is clear that performance on strong SR code trials was significantly elevated ($F(1,731) = 25.84$, $p < 0.001$) during normal delays (≤30 s) and on extended delay (≥40 s) trials, relative to performance on non-closed loop trials of the same duration (control vs CL-strong code, figure 2). Trials with weak SR codes adjusted to 10 s delays by the closed loop paradigm were performed nearly perfectly by all animals (CL-weak codes, figure 2). However, figure 2 also shows that performance was significantly improved on the remaining trials at all delays, (CL-weak code versus control sessions; $F(1,731) = 7.96$, $p < 0.01$) due to the fact that weak code trials were eliminated by the closed loop as a potential source of error on longer delay trials (weak codes, figure 2).

Verification of the MIMO model predictions is shown for trials ≤30 s in which strong or weak SR codes were detected but delays not altered by the closed loop procedure (figure 2 CL-strong code trials <30 s, weak codes shown by inverted triangles). It is clear that performance was maximal when strong codes were detected (CL-strong codes), but markedly decreased on all trials >15 s when weak codes were detected and at risk for error (weak code vs control, $F(1, 731) = 15.61$, $p < 0.001$) as shown in figure 2. It is clear that DNMS performance under normal conditions was a function of two factors: (1) the strength of the SR code, and (2) the coincidence of that code strength with duration of the subsequent randomly assigned delay. Since the delay between SR and NR was unpredictable, strength of SR encoding on any given trial was arbitrary and reflected possible 'anticipation' of the subsequent delay duration. However, as shown previously (Hampson *et al* 2011), if delays were extended beyond previously trained limits (CL-strong code >30 s, figure 2), performance on strong SR code trials also declined in a delay-dependent manner.

3.2. MIMO model stimulation reverses mismatches of SR encoding strength and delay

A unique application of the MIMO model in the closed loop paradigm described above is the ability to substitute electrical stimulation pulses in patterns that mimicked the firing of CA1 outputs predicted from the MIMO model, to facilitate memory under circumstances where there were mismatches in the online generated SR code strength for the duration of the ensuing delay. Such stimulation was used to enhance memory on trials in which the MIMO model detected weak SR codes for trials with delays >10 s (figure 3). Thus substitution of electrical stimulation pulses at the same electrode loci and in the same temporal pattern as strong SR codes reversed mismatches between spontaneously generated SR code strength and the duration of subsequent trial delay (figure 3). This stimulation procedure was capable of facilitating performance in the same manner as MIMO predicted strong SR codes when delays were extended (30–60 s) in the task (figure 3). Trials with interposed CA1 stimulation patterns derived from MIMO generated strong SR codes (stim MIMO model) were significantly increased versus trials on which no stimulation (no stim) was delivered ($F(1,731) = 11.50$, $p < 0.001$). Trials in which stimulation at the same intensity was generated from scrambled MIMO model CA1 coefficients (figure 2) did not differ from no stim trials ($F(1,731) = 2.12$, ns.). Under such circumstances MIMO model

stimulation parameters were applied to the same electrode locations but in a different spatiotemporal pattern (scrambled coefficients, figure 3). The fact that stimulation patterns delivered with scrambled coefficients did not consistently suppress performance as might be expected relates to the fact that only some of the scrambled patterns produced the exact SR codes for the opposite lever, which as shown below (figure 5) was required to drive performance below control levels. In addition, the effectiveness of the stimulation patterns was shown to decline across the same span of extended delays in a manner similar to closed loop trials with MIMO detected strong SR code firing patterns (figure 2). These results demonstrate that substitution of strong SR code patterns of electrical stimulation eliminated trials that were at risk for error when weak SR codes were detected by the MIMO model (figure 3).

3.3. MIMO model derived stimulation replaces lost mnemonic function

The above demonstration that MIMO model stimulation could override the mismatch between anticipated duration of delay and strength of the SR code suggests that such stimulation, if synchronized and delivered at the time of occurrence of the SR, could provide a means of inducing strong SR codes. This was examined under the most severe condition by testing animals when MIMO model predications from hippocampal CA3 inputs were not available online. As in previous studies (Hampson *et al* 1999a) normal operation of hippocampal circuitry was seriously impaired by chronic infusion over a two week period of the glutamatergic transmission blocking agent, MK801 (Collingridge *et al* 1983, Coan *et al* 1987). In animals that were trained to perform the DNMS task, infusion of MK801 unilaterally into the CA3 region (37.5 μg h^{-1}; 1.5 mg ml^{-1}, 0.25 μl h^{-1}) for 14 days produced significant disruptions in performance at all delay intervals and significantly reduced the appearance of strong SR codes detected online by the MIMO model (figure 3). However, since the MIMO model delivered successful SR stimulation patterns in the same animals under normal (nondrug) circumstances, each animal's previously identified effective MIMO stimulation pattern was delivered at the time the animal pressed the sample lever (SR) during testing while MK801 was being chronically infused. MK801 significantly suppressed DNMS performance at all delays compared to control levels ($F(1,416) = 13.37$, $p < 0.001$). However, performance was significantly improved ($F(1,416) = 9.52$, $p < 0.001$) on trials in which CA1 stimulation was delivered with strong SR code patterns, and remained only slightly ($F(1,416) = 5.12$, $p = 0.02$) below control levels. Figure 4 shows that delivery of MIMO stimulation patterns was highly effective in reversing the detrimental effects of the drug and significantly increased performance on all trials with delays >10 s. Even though performance was not elevated back to normal (pre-MK801) levels, delivery of effective MIMO model derived stimulation patterns at the SR significantly reduced the drug-induced deficit.

3.4. Demonstration of specificity of MIMO model derived stimulation patterns

Together, the above demonstrations (figures 2–4) show that detection, imposition and closed loop control based on MIMO-derived ensemble firing patterns control DNMS task behavior by enhancing encoding of the SR sufficient to counteract the effects of the intervening delay interval. It is obvious that such enhanced encoding facilitates making the NR decision, but the specificity of the MIMO model stimulation pattern can be assessed in the same experimental context. A distinct test of the specificity of the information the SR codes and their strength was ascertained by reversing the MIMO stimulation patterns such that the pattern for the *left lever* was delivered when the animal was presented with, and made the SR, on the *right lever* and vice versa. Delivery of the stimulation pattern specific for encoding the lever opposite the one presented and responded to sample, should not only eliminate enhanced encoding of the SR, but should actually impair performance below normal levels due to stimulation induced *miscoding* of information required in the nonmatch

phase to correctly select the NR. Therefore the frequency of errors (match responses) should increase in comparison to trials in which no stimulation occurred. Figure 5 shows that by reversing the MIMO model SR stimulation patterns for the lever presented in the sample phase, performance was reduced below normal levels ($F(1,731) = 12.53$, $p < 0.001$) relative to control trials in which no stimulation occurred. In contrast, trials within the same sessions in which SR codes were delivered appropriate for the lever presented (normal stim) exhibited performance significantly above control levels ($F(1,731) = 15.76$, $p < 0.001$). The results shown in figure 5 support the conclusion that delivery of the opposite SR stimulation pattern was capable of overriding normal encoding tendencies by significantly impairing performance on trials with deliberate mismatches between the SR stimulation pattern and lever position. It is clear that reversed strong SR code patterns had a large impact on performance. To validate the fact that the MIMO stimulation patterns were effective, figure 5 also shows that performance was markedly improved if the same SR stimulation patterns were delivered when the appropriate lever was presented in the sample phase. One final control manipulation for specificity of the MIMO derived stimulation patterns was to delay delivery of the stimulation by 3–5 s after occurrence of the SR (delayed stimulation, figure 5). The results show that if strong SR code stimulation patterns were delayed by more that 3.0 s there was no effect on performance (stim late versus no stim: $F(1,731) = 3.17$, ns).

4. Discussion

The above demonstrations show that neural prostheses employing connections between different neuronal assemblies can be applied to accurately assess and impose effective spatiotemporal task-related firing patterns which can be used for (1) closed loop control of performance (figure 2), (2) electrical stimulation of the same structures in the manner that mimics output of successful task-related signals to facilitate and override instances in which less effective ensemble firing occurs (figure 3), (3) recovery of function when the same ensembles are no longer operative (figure 4) and finally (4) validating whether the facilitative patterns of stimulation are specific to encoding of task-related events necessary for successful performance within specific contexts (figure 5). This type of utility provided by the MIMO model and applied to a well-characterized set of ensemble firings provides one of the first demonstrations in which deciphered nonlinear activation patterns across cell assemblies can be utilized to deliver facilitative electrical stimulation to those same brain regions (Dulay *et al* 2009). Such an approach takes advantage of the fact that input–output relations are all that are required to make the predictions, irrespective of whether those relations reflect mono- or polysynaptic connections. Therefore, even if hippocampal CA3 connectivity to CA1 were not present, the MIMO model could be applied by characterizing input–output relations between dentate gyrus (and/or entorhinal cortex) and CA1 outputs if the former structures remained operative when CA3 was damaged. In addition, by reversing the encoding patterns delivered for critical behavioral events within the task (figure 5), it was possible to test the specificity of the effectiveness of the neural prosthesis for replacing damaged or destroyed connections (Moritz *et al* 2008, Leuthardt *et al* 2009), as shown in figure 4. While some factors remain to be determined as to the basis for the success of this approach (i.e. range of effective stimulation parameters, etc.), and even though opportunities for negative results were provided, the consistency of the outcomes of each of the above test conditions confirm the basic assumption of predictive ensemble encoding as performed by the MIMO model. It was not necessary to understand the basis for firing patterns in CA1 predicted by CA3 in terms of encoded information, even though in the past each structure has been implicated independently in performance of the task from many different perspectives, including hippocampal removal, drug effects and time course of behavioral acquisition (Hampson *et al* 1999a, 2008, Deadwyler *et al* 2007). In addition, previous offline assessments of data from the same DNMS task employing the exact same MIMO model (Zanos *et al* 2008, Song *et al* 2009) provide substantial computational support for the online

predictions of CA1 output firing patterns based on CA3 cell input firing to control online delivery of facilitative SR stimulation patterns (figures 3 and 4).

The efficiency of the cortical prosthesis described here utilizing a MIMO model that predicts firing patterns for successful encoding of task specific information, provides a unique yet feasible approach to constructing prostheses to replace information transmitted between brain structures via nonlinear patterned inputs and outputs (Song *et al* 2007a, 2009). In the case of hippocampal based memories, the above demonstration shows that cognitive processes can be detected in terms of a code that reflects the degree to which information is successfully represented and encoded (figure 2) for retrieval at a later time (Wais *et al* 2006, Wixted 2007, Miller *et al* 2010). The fact that this code can be mimicked by delivery of electrical stimulation in the same spatio-temporal sequence during the to-be-remembered behavioral event, provides a means of (1) improving performance when encoding is deficient (figure 3), (2) replacing memory function when hippocampal processes are compromised (figure 4), and importantly (3) determining the specificity of the electrical stimulation used to mimic the firing patterns that are not present (figures 3 and 5). What is also apparent is that this cortical prosthesis does not require separate probes for delivery of effective neural stimulation, since the stimulation pulses were delivered through the same CA1 array electrodes (figures 1 and 3). Therefore, it is likely that similar assessments could yield further confirmation that MIMO model derived stimulation patterns could be employed as a universal means of recovering lost connections between neural ensembles in other brain regions, as demonstrated here utilizing previously well-characterized hippocampal firing patterns.

Acknowledgments

The authors appreciate the efforts of Andrew Sweatt, Vernell Collins, Rodrigo Espana, Li Hong Shi, Chad Collins and George McLeod. This work was supported by DARPA contracts to SD (N66601-09-C-2080) and to TB (N66601-09-C-2081) (Prog. Dir: COL Geoff Ling), and grants NSF EEC-0310723 to USC (TB), NIH/NIBIB grant no P41-EB001978 to the Biomedical Simulations Resource at USC (VM and TB) and NIH R01DA07625 (SD).

References

Berger TW, et al. Restoring lost cognitive function—hippocampal-cortical neural prostheses. IEEE Eng Med Biol Mag. 2005; 24:30–44. [PubMed: 16248115]

Berger TW, Song D, Chan RHM, Marmarelis VZ. The neurobiological basis of cognition: identification by multi-input, multi-output nonlinear dynamic modeling. Proc IEEE. 2010; 98:356–74.

Brown EN, Barbieri R, Venture V, Kass RE, Frank LM. The time-rescaling theorem and its application to neural spike train data analysis. Neural Comput. 2002; 14:325–46. [PubMed: 11802915]

Coan EJ, Saywood W, Collingridge GL. MK-801 blocks NMDA receptor-mediated synaptic transmission and long term potentiation in rat hippocampal slices. Neurosci Lett. 1987; 80:111–4. [PubMed: 2821457]

Collingridge GL, Kehl SJ, McLennan H. Excitatory amino acids in synaptic transmission in the Schaffer collateral-commissural pathway of the rat hippocampus. J Physiol. 1983; 334:33–46. [PubMed: 6306230]

Daly JJ, Wolpaw JR. Brain-computer interfaces in neurological rehabilitation. Lancet Neurol. 2008; 7:1032–43. [PubMed: 18835541]

Deadwyler SA, Goonawardena AV, Hampson RE. Short-term memory is modulated by the spontaneous release of endocannabinoids: evidence from hippocampal population codes. Behav Pharmacol. 2007; 18:571–80. [PubMed: 17762525]

Deadwyler SA, Hampson RE. Ensemble activity and behavior: what's the code? Science. 1995; 270:1316–8. [PubMed: 7481817]

Deadwyler SA, Hampson RE. The significance of neural ensemble codes during behavior and cognition. Annu Rev Neurosci. 1997; 20:217–44. [PubMed: 9056713]

Deadwyler SA, Hampson RE. Differential but complementary mnemonic functions of the hippocampus and subiculum. Neuron. 2004; 42:465–76. [PubMed: 15134642]

Deadwyler SA, Hampson RE. Temporal coupling between subicular and hippocampal neurons underlies retention of trial-specific events. Behav Brain Res. 2006; 174:272–80. [PubMed: 16876266]

Dulay MF, Murphey DK, Sun P, David YB, Maunsell JH, Beauchamp MS, Yoshor D. Computer-controlled electrical stimulation for quantitative mapping of human cortical function. J Neurosurg. 2009; 110:1300–3. [PubMed: 19061348]

Hampson RE, Deadwyler SA. Temporal firing characteristics and the strategic role of subicular neurons in short-term memory. Hippocampus. 2003; 13:529–41. [PubMed: 12836920]

Hampson RE, Jarrard LE, Deadwyler SA. Effects of ibotenate hippocampal and extrahippocampal destruction on delayed-match and -nonmatch-to-sample behavior in rats. J Neurosci. 1999a; 19:1492–507. [PubMed: 9952425]

Hampson, RE.; Simeral, JD.; Berger, TW.; Song, D.; Chan, RHM.; Deadwyler, SA. Cognitively relevant recording in hippocampus: beneficial feedback of ensemble codes in a closed loop paradigm. In: Vertes, RP.; Stackman, RW., editors. Electrophysiological Recording Techniques. New York: Humana Press; 2011. p. 215-39.

Hampson RE, Simeral JD, Deadwyler SA. Distribution of spatial and nonspatial information in dorsal hippocampus. Nature. 1999b; 402:610–4. [PubMed: 10604466]

Hampson, RE.; Simeral, JD.; Deadwyler, SA. Neural population recording in behaving animals: constituents of the neural code for behavior. In: Holscher, C.; Munk, MH., editors. Neural Population Encoding. Cambridge: Cambridge University Press; 2008. p. 74-94.

Isa T, Fetz EE, Müller KR. Recent advances in brain–machine interfaces. Neural Netw. 2009; 22:1201–2. [PubMed: 19840893]

Jarosiewicz B, Chase SM, Fraser GW, Velliste M, Kass RE, Schwartz AB. Functional network reorganization during learning in a brain–computer interface paradigm. Proc Natl Acad Sci USA. 2008; 105:19486–91. [PubMed: 19047633]

Legenstein R, Chase SM, Schwartz AB, Maass W. A reward-modulated hebbian learning rule can explain experimentally observed network reorganization in a brain control task. J Neurosci. 2010; 30:8400–10. [PubMed: 20573887]

Leuthardt EC, Schalk G, Roland J, Rouse A, Moran DW. Evolution of brain–computer interfaces: going beyond classic motor physiology. Neurosurg Focus. 2009; 27:E4. [PubMed: 19569892]

Marmarelis, VZ. Nonlinear Dynamic Modeling of Physiological Systems. Hoboken, NJ: Wiley; 2004.

Marmarelis VZ, Berger TW. General methodology for nonlinear modeling of neural systems with Poisson point-process inputs. Math Biosci. 2005; 196:1–13. [PubMed: 15963534]

Marmarelis VZ, Orme ME. Modeling of neural systems by use of neuronal modes. IEEE Trans Biomed Eng. 1993; 40:1149–58. [PubMed: 8307599]

Miller KJ, Schalk G, Fetz EE, den Nijs M, Ojemann JG, Rao RP. Cortical activity during motor execution, motor imagery, and imagery-based online feedback. Proc Natl Acad Sci USA. 2010; 2:4430–5. [PubMed: 20160084]

Moritz CT, Perlmutter SI, Fetz EE. Direct control of paralyzed muscles by cortical neurons. Nature. 2008; 456:639–42. [PubMed: 18923392]

Simeral, JD.; Hampson, RE.; Deadwyler, SA. Behaviorally relevant neural codes in hippocampal ensembles: detection on single trials. In: Baudry, M.; Bi, X.; Schreiber, S., editors. Synaptic Plasticity: From Basic Mechanisms to Clinical Applications. Cambridge, MA: MIT Press; 2005. p. 459-76.

Song D, Chan RH, Marmarelis VZ, Hampson RE, Deadwyler SA, Berger TW. Nonlinear dynamic modeling of spike train transformations for hippocampal-cortical prostheses. IEEE Trans Biomed Eng. 2007a; 54:1053–66. [PubMed: 17554824]

Song D, Chan RH, Marmarelis VZ, Hampson RE, Deadwyler SA, Berger TW. Statistical selection of multiple-input multiple-output nonlinear dynamic models of spike train transformation. Conf Proc IEEE Eng Med Biol Soc. 2007b; 1:4727–30.

Song D, Chan RH, Marmarelis VZ, Hampson RE, Deadwyler SA, Berger TW. Nonlinear modeling of neural population dynamics for hippocampal prostheses. Neural Netw. 2009; 22:1340–51. [PubMed: 19501484]

Truccolo W, Eden UT, Fellows MR, Donoghue JP, Brown EN. A point process framework for relating neural spiking activity to spiking history, neural ensemble, and extrinsic covariate effects. J Neurophysiol. 2005; 93:1074–89. [PubMed: 15356183]

Velliste M, Perel S, Spalding MC, Whitford AS, Schwartz AB. Cortical control of a prosthetic arm for self-feeding. Nature. 2008; 453:1098–101. [PubMed: 18509337]

Wais PE, Wixted JT, Hopkins RO, Squire LR. The hippocampus supports both the recollection and the familiarity components of recognition memory. Neuron. 2006; 49:459–66. [PubMed: 16446148]

Wang W, Chan SS, Heldman DA, Moran DW. Motor cortical representation of hand translation and rotation during reaching. J Neurosci. 2010a; 30:958–62. [PubMed: 20089904]

Wang W, Collinger JL, Perez MA, Tyler-Kabara EC, Cohen LG, Birbaumer N, Brose SW, Schwartz AB, Boninger ML, Weber DJ. Neural interface technology for rehabilitation: exploiting and promoting neuroplasticity. Phys Med Rehabil Clin N Am. 2010b; 21:157–78. [PubMed: 19951784]

Witter, MP.; Amaral, DG. The Rat Nervous System. 3. Paxinos, G., editor. San Diego, CA: Academic; 2004. p. 637-87.

Wixted JT. Dual-process theory and signal-detection theory of recognition memory. Psychol Rev. 2007; 114:152–76. [PubMed: 17227185]

Zanos TP, Courellis SH, Berger TW, Hampson RE, Deadwyler SA, Marmarelis VZ. Nonlinear modeling of causal interrelationships in neuronal ensembles. IEEE Trans Neural Syst Rehabil Eng. 2008; 16:336–52. [PubMed: 18701382]

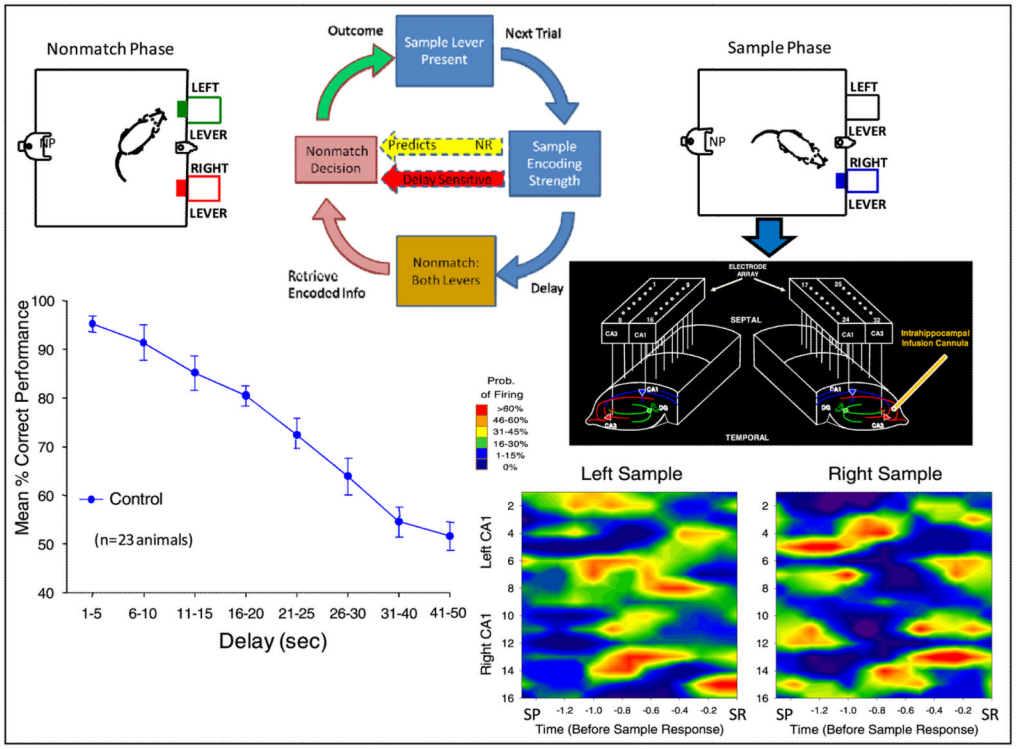

Figure 1.

Top, diagram of DNMS task (clockwise from top). Sample phase starts with single lever extended in one position. SR encoding strength (recorded via array electrodes in CA3 and CA1, center right) predicts delay-sensitive (red arrow) nonmatch response (left). Following random delay, both levers are extended in nonmatch phase. Nonmatch decision requires animal to press lever opposite to SR. Spatiotemporal patterns of ensemble firing are illustrated in color contour maps showing differential firing to left versus right SRs which occurred for 3.0–5.0 s following sample lever presentation (SP). Maps depict firing rate of neurons (vertical axis) by time (horizontal axis) for same 5.0 s period. Overall feedback loop for trials is closed by behavioral outcome based on correct or error recall of sample lever position. Bottom left: performance (mean percentage correct ± SEM) curve illustrates sensitivity of behavior to duration of delay interval under control conditions (n = 23). A unilateral cannula located in CA3 is shown next to array to indicate the site of drug infusion to alter task-related firing (figure 4).

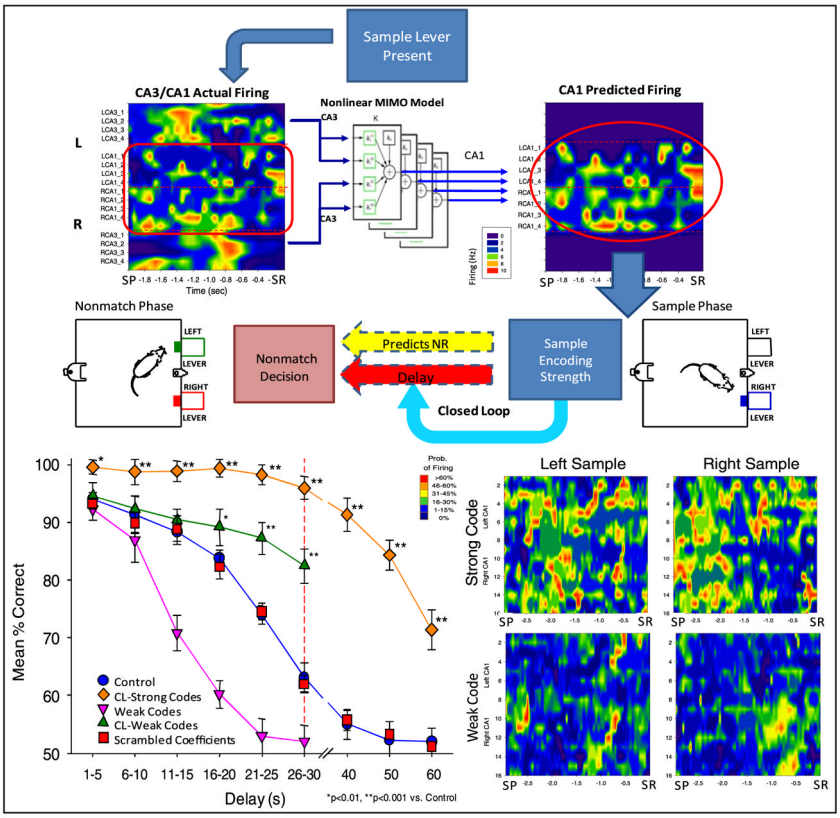

Figure 2.

Closed loop feedback using MIMO identification of SR encoding strength to control DNMS performance. Top: CA3 and CA1 neuronal firing (contour, left) analyzed via MIMO model (center) predicts CA1 firing patterns (contour, right). Strength of SR code in CA1 *during sample phase* predicts behavioral outcome (nonmatch decision) based on prior correlation of firing pattern with success. Closed loop (light blue arrow) reduces (CL-weak codes), or lengthens (CL-strong codes) the delay duration *on the same trial* to validate MIMO model prediction of strength of the SR code. Bottom right: mean strong and weak code patterns of probability of neural firing at each neuron position (array recording site) and time relative to SR. Color contours scaled from blue (<10%) to red (>60%) according to probability of neural firing on a single trial. Bottom left: mean DNMS performance across animals (n = 15) compares performance on closed loop MIMO model-detected strong (CL-strong codes) and weak (CL-weak codes) SR codes to non-closed loop trials (control). Performance on non-closed loop trials with detected weak codes is displayed as well (weak codes). Performance on trials in which MIMO coefficients were scrambled (scrambled coefficients) is also shown.

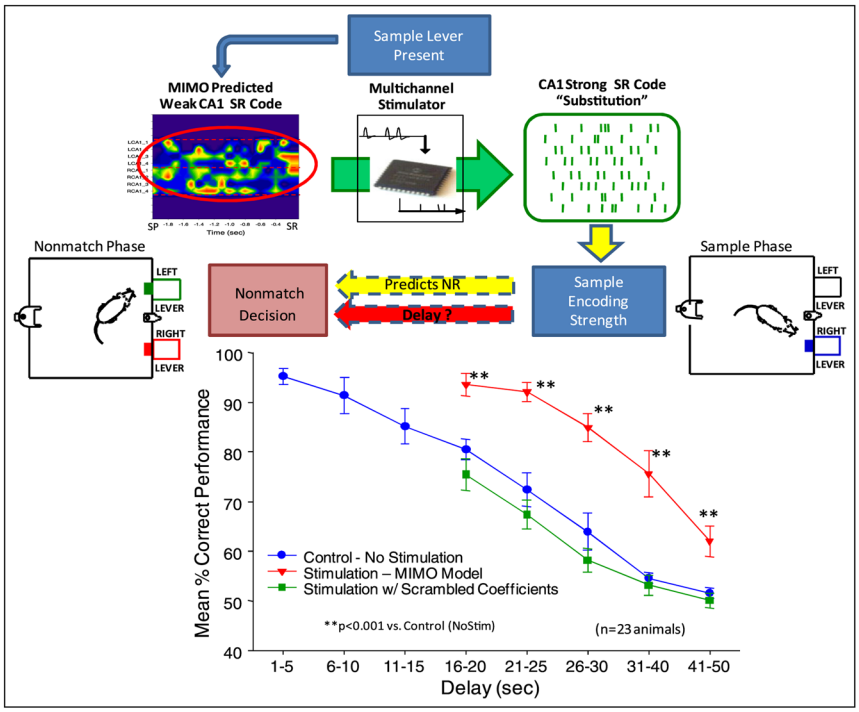

Figure 3.

MIMO model controlled stimulation codes. Top: prediction of 'weak' SR encoding in CA1 via MIMO model results in CA1 electrical stimulation with spatio-temporal patterns corresponding to strong SR code (green raster 'substitution', top right) predicted by prior closed loop MIMO model applications (figure 2). CA1 stimulation consisted of biphasic electrical pulses (0.5–2.0 V, 10–50 μV, 0.5 s duration) delivered no more than once per 50 ms per channel, delivered on trials with delay durations of 15–50s. Bottom: comparison of mean DNMS performance (% correct ±SEM) across animals (n = 23) on trials with interposed CA1 stimulation patterns derived from MIMO generated strong SR codes (stim MIMO model) vs. trials on which no stimulation (no stim) was delivered. Trials in which stimulation at the same intensity was generated from scrambled MIMO model CA1 coefficients (figure 2) are also shown.

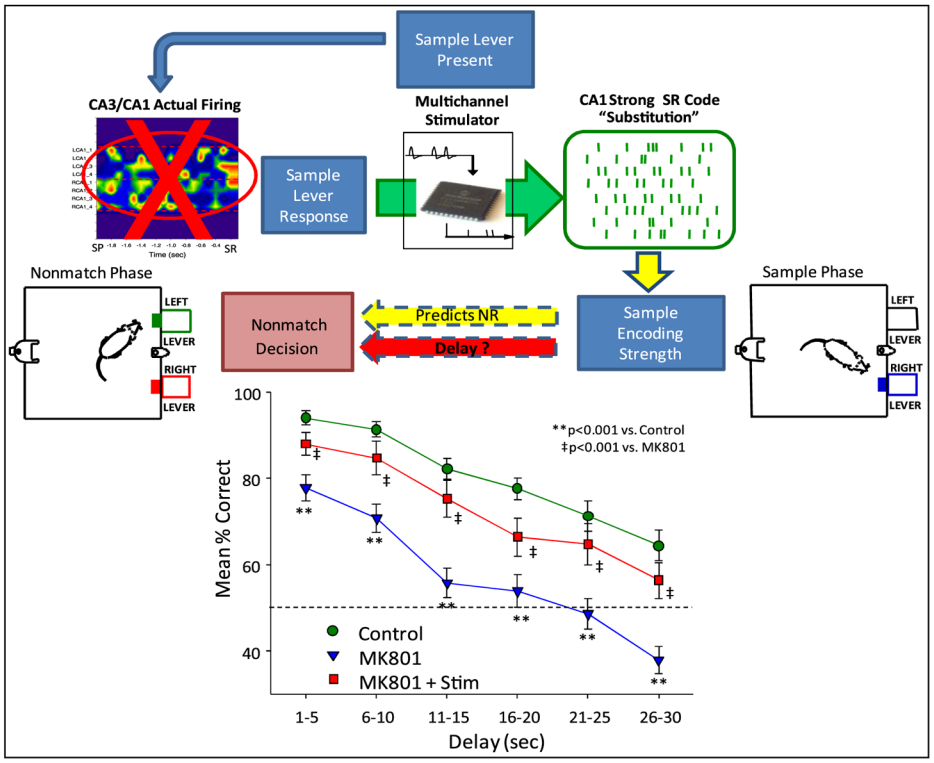

Figure 4.

MIMO model repair of hippocampal encoding with previously effective CA1 stimulation patterns delivered at the time of the SR. Top: intrahippocampal infusion (see figure 1, inset center right, cannula shown entering CA3 next to electrode array on right) of glutamatergic antagonist MK801 for 14 days suppressed MIMO derived ensemble firing in CA1 and CA3 (red 'X', left). Strong SR code patterns derived from previous DNMS trials were delivered bilaterally to the same CA1 locations when the SR occurred in the sample phase. Bottom: mean percentage correct (±SEM) performance (n = 5 animals) summed over all conditions, including vehicle-infusion (control) without stimulation, MK801 infusion (MK801) without stimulation, and MK801 infusion with the CA1 stimulation (substitute) pattern (MK801 + Stim).

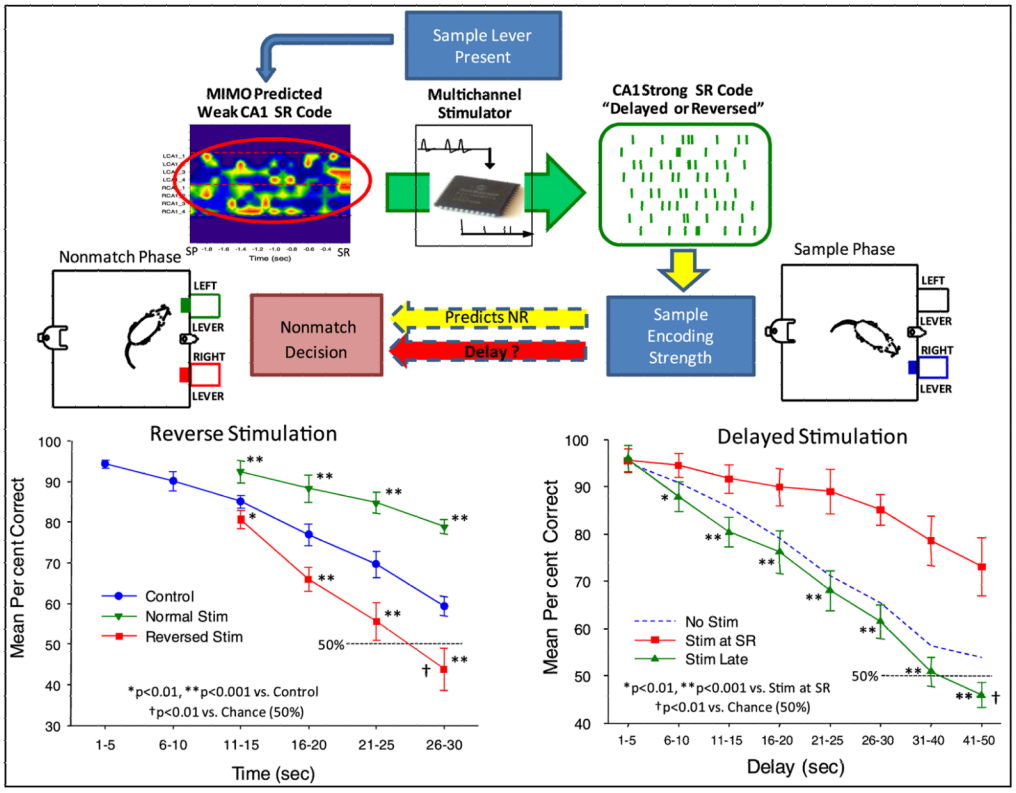

Figure 5.

Reverse stimulation to verify specificity of closed loop MIMO model stimulation. Top: validity of CA1 'strong SR code' patterns determined by delivering stimulation patterns appropriate for the opposite type of DNMS trial ('reversed') or by varying the time at which stimulation was delivered relative to the occurrence of the SR ('delayed'). Bottom left: DNMS trials in which the SR code for the opposite lever was delivered (reversed stim) and compared with trials within the same sessions in which SR codes were delivered appropriate for the lever presented (normal stim) as well as control (no stimulation) trials. Bottom right: DNMS delay curves for animals stimulated with MIMO model generated strong SR codes either at the time of the SR (stim at SR) or commencing 3–5 s after the SR (stim late).